Analysis of the outer divertor hot spot activity in the protection video camera recordings at JET

A. Drenik[1, 2], S. Brezinsek[3], P. Carvalho[4], V. Huber[3], N. Osterman[2], G. F. Matthews[5], M. Nemec[6] and the JET contributors[*]

[1] Max-Planck-Institut für Plasmaphysik, Boltzmannstr. 2, 85748 Garching b. München, Germany,
[2] Jožef Stefan Institute, Jamova ulica 39, SI-1000 Ljubljana, Slovenia,
[3] Forschungszentrum Jülich GmbH, Institut für Energie- und Klimaforschung – Plasmaphysik, Partner of the Trilateral Euregio Cluster (TEC), 52425 Jülich, Germany,
[4] Instituto de Plasmas e Fusão Nuclear, IST, Av. Rovisco Pais, 1049-001 Lisboa, Portugal,
[5] Culham Centre for Fusion Energy, Abingdon, Oxon, OX14 3DB, United Kingdom,
[6] University of Ljubljana, Faculty of Electrical Engineering, Tržaska cesta 25, SI-1000 Ljubljana, Slovenia,
***** See the author list of "X. Litaudon *et al* 2017 *Nucl. Fusion* 57 102001"

Abstract

Hot spots on the divertor tiles at JET result in overestimation of the tile surface temperature which causes unnecessary termination of pulses. However, the appearance of hot spots can also indicate the condition of the divertor tile surfaces. To analyse the behaviour of the hot spots in the outer divertor tiles of JET, a simple image processing algorithm is developed. The algorithm isolates areas of bright pixels in the camera image and compares them to previously identified hot spots. The activity of the hot spots is then linked to values of other signals and parameters in the same time intervals. The operation of the detection algorithm was studied in a limited pulse range with high hot spot activity on the divertor tiles 5, 6 and 7. This allowed us to optimise the values of the controlling parameters. Then, the wider applicability of the method has been demonstrated by the analysis of the hot spot behaviour in a whole experimental campaign.

Keywords: JET; ITER-like wall; plasma-wall interaction; image analysis

1. Introduction

JET is currently the largest operating tokamak, capable of running plasma pulses with a flat top duration of over 10 seconds and a routinely achievable combined heating power over 15 MW[1]. As a consequence, plasma wall interaction can, if uncontrolled, cause significant damage to the plasma facing components. This issue has become especially important after the installation of the ITER-like wall (ILW)[2], where the carbon-fibre composite (CFC) tiles in the divertor were replaced with bulk tungsten (W) and W-coated CFC tiles which impose stricter heat load restrictions. In order to prevent recrystallization of the bulk W tile, and the delamination of the W coatings, the surface temperature must be kept below 1200 °C[3,4]. To prevent such damage to the plasma facing components (PFCs) due to excessive heat loads, JET relies on an array of video cameras, *protection cameras*, which monitor the temperature of the plasma facing surfaces[5–8]. The field of view of each protection camera is split into pre-determined regions of interest (ROIs). Each ROI provides a temperature signal, which represents the highest temperature (i.e. coming from the pixel with the highest intensity) within the ROI. A selected range of the temperature signals is included into the JET

protection system. In the case that a temperature from an observed ROI exceeds the threshold value, defined by the plasma facing material of the ROI, for more than 0.4 seconds, a high temperature alarm is triggered and the pulse is stopped to prevent further damage to the plasma facing component[9]. The frequency of high temperature alarms, triggered by the signals from the protection cameras in the second ILW campaign is plotted in Fig. 1 and it shows that the majority of the alarms are related to the high temperatures on three sections of the divertor: tile 5 (bulk W horizontal target), tiles 6 and 7 (horizontal and vertical W-coated CFC targets in the outer divertor), and the main chamber (MC) components.

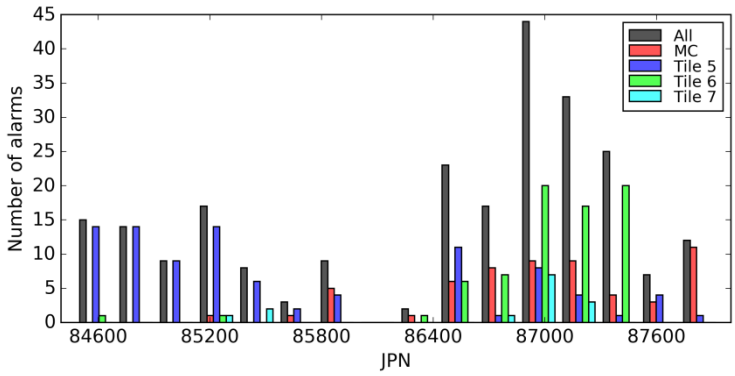

Figure 1. Frequency of high temperature alarms triggered by the protection cameras at JET, in the corresponding to the second ILW campaign

However, high temperature alarms are also triggered by hot spots – narrowly localized areas whose temperature is significantly higher than the underlying surface[5]. In such cases, the high value of the temperature signal does not represent the true temperature of the plasma component and the pulse is terminated on the basis of a false-positive alarm. On the other hand, the appearance of hot spots might also indicate accumulation of debris or molten material on the surface or delamination of the divertor tile coating. Material with poor adhesion to the surface can be mobilized which can lead to dust production and increased influx of impurities into the plasma[10]. To reduce the frequency of false positive alarms from the thermal protection system, recent efforts have been invested in the characterisation of appearance, and cataloguing hotspots in the field of view of the protection cameras[11]. The recognition of hot spots, at the present moment, is being done by hand, however the aim is to develop a method of automated detection of hot spots.

Several approaches to automated detection of hot spots in various fields of plasma-surface interaction have been developed[12], including algorithms for hot spot detection in the recordings of IR cameras in Tore supra[13,14] and JET[15]. However, because the IR cameras have a different viewing angle than the protection cameras, the information about the hotspots in the recorded images cannot be directly transferred to the ROIs of the protection cameras. On the other hand, because the visual video signals carry significantly less detailed information about the surface temperature, the already developed algorithms cannot be applied directly.

In this paper, we present a simple algorithm for detection of hot spots in the recordings of protection cameras, with the future goal of the integration into the JET's thermal protection software suite[11]. Beside detecting hot spots, the algorithm also tracks their activity, which then allows for the evaluation of the hot spot activity over time and relating it to different plasma parameters. The detection and recognition algorithm is presented in the following section of the paper, while the results, obtained from applying the algorithm to the video recordings from the second ILW campaign are presented in the 3rd section.

2. Detection and recognition of hot spots

The detection of hot spots is based on identifying isolated areas clusters of bright pixels in the camera images, and tracking their activity through successive frames. Apart from isolating the bright pixel clusters, the main part of the algorithm is the criterion which determines whether one such clusters corresponds to any of the previously recognized hot spots, based on its position and size in the camera image.

The hot spots are stored in a hot spot catalogue as lists of (x,y) coordinates of pixels which make up the isolated clusters of bright pixels. A cluster of pixels *A* is found to correspond to a catalogue entry *B* based on two criteria:

1. The surface area of the overlap between the two pixel clusters, *O*, must be greater than a certain fraction (`min_overlap`) of the surface area of the smallest of the two clusters. This ensures that the two clusters occupy a sufficiently similar area in the camera image.

   The overlapping area between the two clusters, *O*, is the intersection between the two lists of clusters. The area size of a pixel cluster is defined as the number of pixels it comprises. Thus, the size of the overlapping area is the number of pixels shared between pixel clusters *A* and *B*. The evaluation of C_1 is then:

   $$C_1(A,B) = \begin{Bmatrix} True; S(O) \geq \text{min\_overlap} \cdot min(S(A), S(B)) \\ False; S(O) < \text{min\_overlap} \cdot min(S(A), S(B)) \end{Bmatrix}$$

   Where $S(A)$, $S(B)$and $S(O)$ are the surface areas of pixel clusters *A* and *B*, and of their overlapping area.

2. The surface area of the largest among the pixel clusters should not exceed the surface area of the smallest by a certain factor (`max_oversize`). This ensures that the size of the two clusters is sufficiently similar. The evaluation of C_2 is:

   $$C_2(A,B) = \begin{Bmatrix} True; \frac{S(A)}{S(B)} \geq \frac{1}{\text{max\_oversize}} \ \ and \ \ \frac{S(A)}{S(B)} \leq \text{max\_oversize} \\ False; \frac{S(A)}{S(B)} < \frac{1}{\text{max\_oversize}} \ \ or \ \ \frac{S(A)}{S(B)} > \text{max\_oversize} \end{Bmatrix}$$

The correspondence between the two clusters is then finally evaluated as:

$$C(A,B) = C_1(A,B) \ and \ C_1(A,B)$$

The aim of these correspondence criteria is to enable the recognition of the same hot spot in different frames of the video recording, in which the image of the hot spot does not always result in the same cluster of bright pixels due to fluctuations in its temperature or noise (e.g. bright pixels due to neutrons[6]).

The process of detecting hot spots in the video recording from a single plasma pulse is as follows:

1. In each frame, the image is binarised (i.e. pixels with a brightness above a certain `threshold` are set to 1, the others to 0).

2. Isolated clusters of two or more bright pixels are indexed as lists of coordinates of the pixels they comprise.

3. Each bright pixel cluster is compared against a catalogue of previously identified hot spots, using the set values of `min_overlap` and `max_oversize`. If a cluster is found to correspond to a hot spot definition, that hot spot is marked as active in the running frame. If the cluster does not correspond to any of the hot spot definitions in the catalogue, it is stored in a catalogue of temporary hot spots. Unlike the verified hot spots, the hot spots in the temporary catalogue have a stricter `min_overlap` (0.9) and `max_oversize` (1.1) when compared against pixel clusters in future frames. When found to correspond to a bright pixel cluster in a future frame, the definition of a temporary hot spot is updated to include all of the pixels from the cluster.

4. After all frames in the video recording have been processed, the temporary hot spots are filtered with the requirement of a minimum un-interrupted duration of activity over a certain number of frames (`min_persistence`). The sufficiently persistent hot spots are then further checked for correspondence against one another, this time with the `min_overlap` and `max_oversize` set for the hot spots in the established catalogue. Finally, the new hot spots are checked for correspondence against the hot spots in the established catalogue. Any hot spots not corresponding to previous entries are then added to the catalogue of established hot spots. The periods of the activity of existing and newly added hot spots are filtered with the requirement of minimum duration of two consecutive frames.

The operation of the algorithm is thus fully determined with four parameters: `threshold`, `min_persistence`, `min_overlap` and `max_oversize`.

The input data for the detection algorithm are raw video recordings. In case of the JET protection cameras, these are 288 pixel by 720 pixel monochrome videos with an 8 bit resolution, recorded at 49 frames per second. The pixel brightness, used in the detection algorithm, is the non-calibrated digital level of the video recording, rather than the surface temperature. However, by using the raw data, the analysis is not limited to the calibrated

areas, but can be performed in the entire viewing field of the camera. Moreover, by not relying on temperature calibration, uncertainties that would arrive from hot spots lying between the borders of different areas, are also avoided.

The impact of these parameters was evaluated by processing the video recording from the KL1-P4DB camera, in a limited pulse range (ranges JPN 84758 – 84784 and 84955 – 84964, 87060 – 87095 and 87208 – 87240) in which high temperature alarms were being triggered with significant frequencies, by signals of that same camera, related to tiles 5, 6 and 7 respectively. The hot spot activity was analysed with `threshold` ranging from 80 to 254, and `min_persistence` ranging from 3 to 5. The parameters related to the recognition of existing hot spots were set for a relatively strict filter. The parameter `min_overlap` was set at 0.9 and `max_oversize` was set at 1.2.

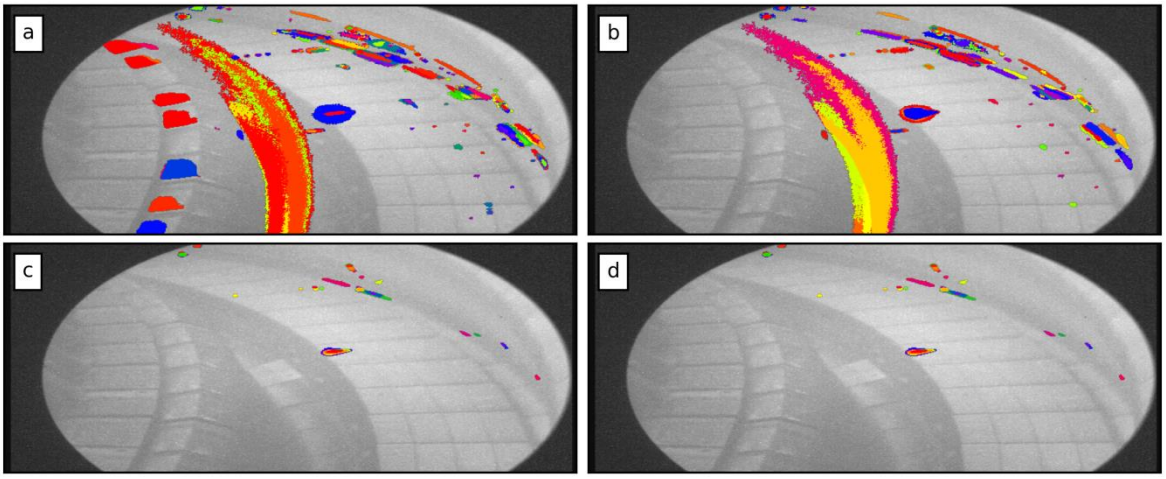

Figure 2. Catalogues of indexed hot spots at a: `min_persistence` = 3 and `threshold` = 80, b: `min_persistence` = 4 and `threshold` = 80, c: `min_persistence` = 4 and `threshold` = 220, d: `min_persistence` = 4 and `threshold` = 250

The impact of the variation of the parameters is shown, in part, in Figure 2. At low `threshold` values, several features are detected which are not related to hot spots, such as the large, solid area inboard of tile 5, seen in Figs. 2a and b. The large areas most likely attain the necessary brightness during disruptions, MARFEs or reflections of the plasma radiation, bremsstrahlung, etc. from the neighbouring surfaces. This issue appears at all values of `min_persistence`, however is completely eliminated by raising `threshold` to 110 or 100 for `min_persistence` values of 3 and 4, and 5 respectively. At the lower `threshold` values, large solid areas on tile 4 are also indexed as hot spots (Fig. 2a), however only at values of for `min_persistence` 3. By applying increasingly stricter detection criteria (Figs a c and d), the number of detected features is further reduced (Fig. 2c). The remaining features all exhibit same visual characteristics as hot spots identified by preliminary manual analysis, i.e. they are relatively small, ellipsoid shapes, distributed mainly in an area parallel to the edge of tile 5.

The number of detected hot spots is also affected by the parameters which control the hot spot recognition criteria, `min_overlap` and `max_oversize`.. To evaluate the impact of the recognition criteria, the camera recordings were processed with relatively strict settings of the recognition parameters, and the resulting hot spots catalogues were then re-processed with more relaxed recognition criteria, listed in Table 1.

To estimate the overlapping hot spot definitions in the resulting catalogues, we observe the so-called average pixel coverage. The average pixel coverage is calculated as the average number of hot spot definitions in which each pixel in the camera image. For clarity, this statistic does not include the pixels which are not covered by any of the hot spot definitions in the catalogue. In the ideal case, when none of the hot spot definitions are overlapping, the average pixel coverage would thus be equal to 1, whereas higher values indicate overlapping hot spot definitions. A relatively large fraction of overlapping hot spots in the catalogue plots of Fig. 3 indicate that the correspondence criteria are indeed too stringent as the algorithm fails to recognize some of the hot spots. Then, the hot spot definitions are unnecessarily detailed and the same actual hot spot is covered by several catalogue entries, varying only little in size and position. With the most relaxed filter version, the average pixel coverage is reduced by approximately a factor of 3 compared to the most stringent version of the filter however the average pixel coverage is never exactly at 1, meaning that overlapping of hot spot definitions cannot be completely avoided. Moreover, when the criteria are too relaxed, however, several hot spots can be merged in a single, large area, which can also hinder the analysis of the hot spot activity. The optimal compromise between overly detailed definitions and over-merging was found to be at the filter version 3. The comparison between the detected hot spots with the strictest filter (version 0) and the chosen filter version 3 is also presented in Fig. 4, which shows a close up on a cluster of hot spots, as detected with both versions of the filter. With the stringent filter, the algorithm detects several hot spots of different sizes on the same part of the camera image whereas with the relaxed filter settings, the smaller hot spots are included in the definitions of the larger ones with which they overlap. Accordingly, the number of detected hot spots in that area is reduced from 42 to 15.

Table 1: Filter settings used in analysis of the operation of the algorithm

Filter version	`min_overlap`	`max_oversize`
0	0.9	1.2
1	0.8	1.6
2	0.8	2.5
3	0.6	2.5
4	0.5	4

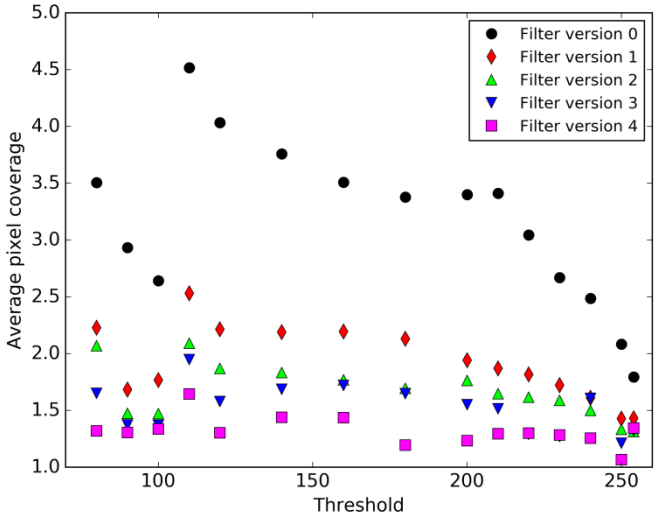

Figure 3. Average coverage of pixels by hot spot definitions, as a function of the `threshold` value, at the `min_persistence` value of 4. The break in the trend at `threshold` = 110 is due to the detection of large solid areas at lower threshold values, which distort the statistic by contributing a very large number of pixels.

Figure 4. Close up to a cluster of hot spots on tile 6 at filter version 0 (a) and the chosen filter version 3 (b), at the `threshold` of 180 and `min_persistance` at 4. With the version 0, the area is covered by 42 catalogue hot spot entries, while in the version 3 the number is reduced to 15.

3. Analysis of the hot spot activity

The appearance and activity of the outer divertor hot spots was analysed in the same data set as the high temperature alarms presented in Figure 1, which represents the second ILW campaign. As in the previous section, the source of data was the protection camera KL1-P4DB[5,7], looking at the outer divertor. Based on the study of the impact parameter variation described in the previous section, three of the four parameters which control the detection and recognition algorithm were fixed. The value of `min_persistance` set at 4, `min_overlap` at 0.6 and `max_oversize` at 2.5. The value of `threshold` was varied between 180 and 250.

The preliminary analysis has shown that plasma operation with less than 2.5 MW NBI heating does not result in hot spot activity. Based on that, the dataset was limited to recordings during which the NBI heating power was above 2.5 MW. This way, the computing time was reduced, as well as the risk of detecting bright features that were not related to plasma-wall interaction (e.g. disruptions in L-modes). A total of 1749 video recordings were analysed, with the average running time of 14.1 s per pulse. The analysis was performed on the JET analysis

cluster computers, and the average processing time was 53.8 ms per frame. The catalogue images are shown in Fig. 5, for some of the `threshold` values. As expected from the findings of the previous section, all of the used threshold values were sufficiently high to avoid indexing any obviously non-hot spot features or large illuminated areas (Figs. 2a and 2b) in the hot spot catalogues. Nevertheless, certain entries in the catalogues can be attributed to features on the divertor target plates which exhibit hot spot like temperature behaviour, but are not *de facto* hot spots. These are the Langmuir probe tips, seen along a straight line across tile 5, and the exposed tungsten lamella on the inboard side of tile 5, which was deliberately melted in a dedicated experiment[16,17]. The number of detected Langmuir probe tips is reduced considerably at the highest `threshold` value, but the exposed lamella persists all throughout the range as the surface was at the melting point of tungsten whereas the signal of the protection camera saturates at lower surface temperatures[8]. It can be also noted that, apart from the deliberately exposed surfaces, very little hot spots were detected on the surface of tile 5, which is not surprising as the surfaces of bulk-W tiles are expected to be more resilient than W-coating on CFC tiles, and for geometrical reasons, accumulation of debris is not expected to be the most prominent in this part of the divertor[18].

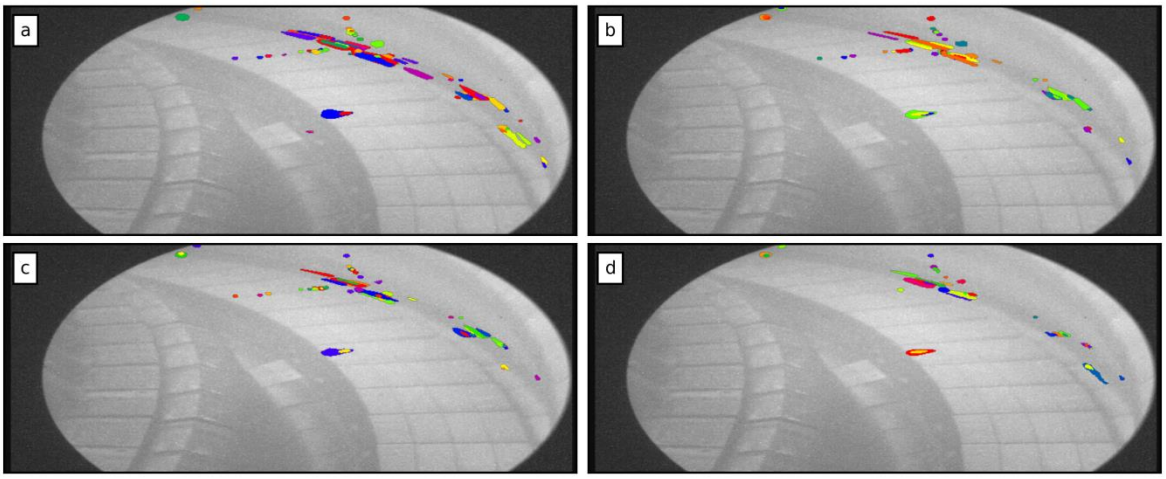

Figure 5. Catalogue images of hot spots detected in the demonstration pulse range, for `threshold` values 180 (a), 210 (b), 230 (c) and 250 (d)

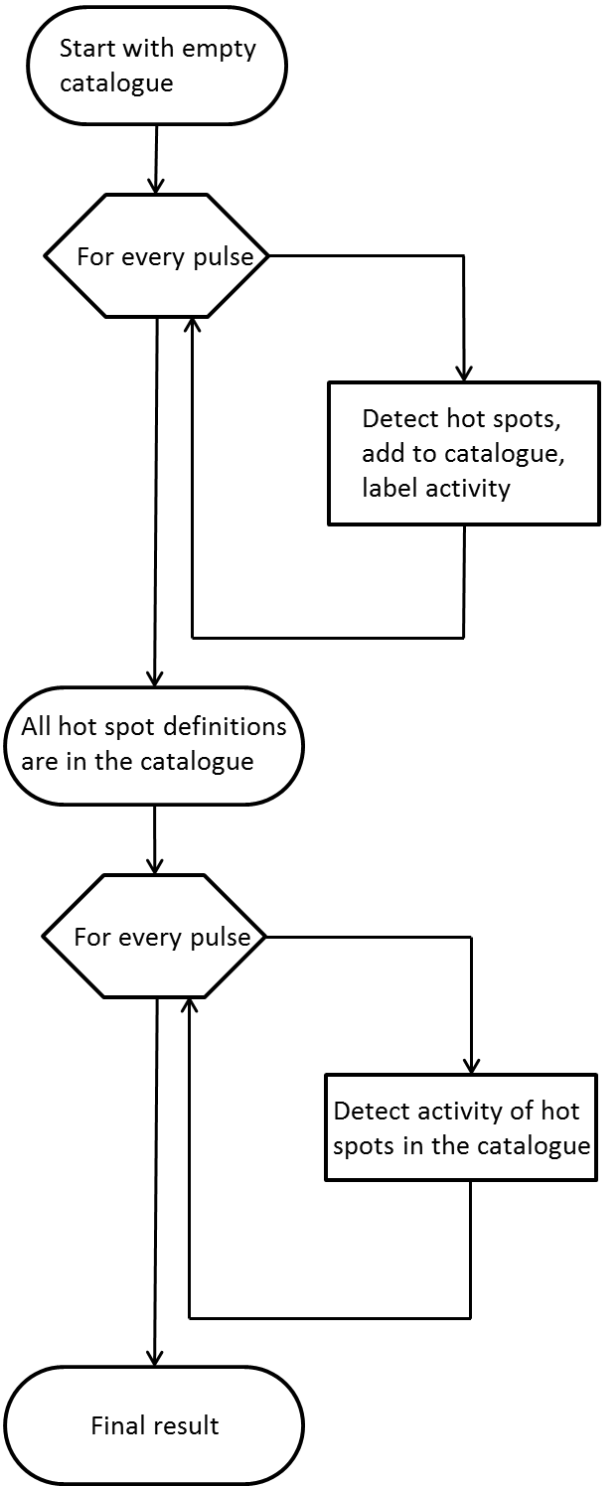

Figure 6. Flowchart of the processing of all of the pulses in the campaign. The processing is done twice, keeping the same catalogue of hot spot definitions.

For each `threshold` value, the analysis was performed twice in a row, keeping the same catalogue of identified hot spots for the 2nd run, as shown in Fig. 6. The 2nd run of the analysis was thus performed from the beginning with a full catalogue of detected hot spots. In order to register activity of an existing hot spot, the required persistence is only 2 consecutive frames in the video recording, opposed to the 4 required to register a new hot spot in the catalogue, therefore the 2nd run show the results of a more sensitive detection of activity. This is

illustrated in Fig. 7, which shows histograms of first appearance of the hot spots in the first and second run, at `threshold` values 180, 210, 230 and 250. First appearance denotes the pulse number in the pulse range at which the activity for a particular hot spot was first registered. At each `threshold` value, the first observed activity in the second run tends to gravitate towards lower pulse numbers, compared to the first one. Because of this higher sensitivity, the results discussed in the remainder of the text are going to be obtained from the 2nd runs.

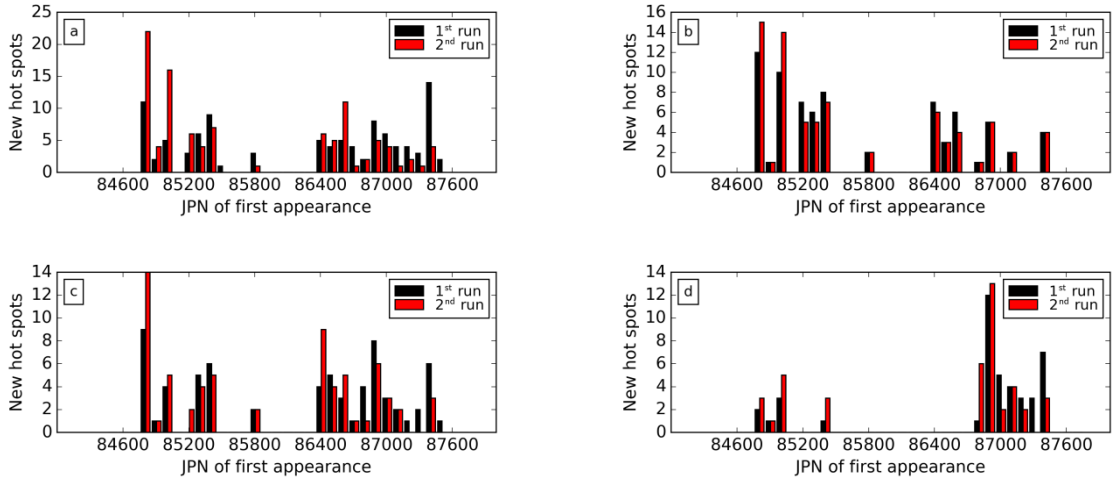

Figure 7. First noted hot spot activity in the first and second run, for `threshold` values 180 (a), 210 (b), 230 (c) and 250 (d)

Keeping track of the activity of each individual hot spot makes it possible to correlate it to various plasma parameters. As mentioned above, the activity of the hot spots is caused by plasma-wall interaction, i.e. a hot spot becomes active when there is sufficient heat flux from the plasma towards the plasma-facing surface. Thus, the parameter which is linked most strongly to the hot spot activity would be the position of the strike point (where the heat flux is the highest), and the plasma heating power. The observed parameters were therefore the R and Z coordinate of the outer strike point, because the protection camera KL1-P4DB is focused at the outer divertor, and the NBI heating power, because the auxiliary heating power is dominated by the neutral beam injection.

For each individual hot spot, the values of the observed parameters were collected from the periods of its registered activity. This compiled database allows for the determination of the conditions which result in a hot spot activity. For each coordinate, the data points were distributed in 20-bin histograms. The central coordinate value was defined as the centre of the bin with the highest count, while the lower and upper limits of the outer strike point coordinates were defined as the first bin respectively left and right of the central bin, which showed a count lower than 5 % of the maximum count. These boundaries of the R and Z coordinate of the outer strike point define *activation areas* for each hot spot. The NBI power data points were treated the same way. In this case, the minimal NBI power required for the activity of a hot spot was defined as the lower boundary.

Identifying the activation areas of the hot spots makes it possible to study their behaviour based on their location, as seen in Fig 8, which shows the first appearance of hot spots grouped by the divertor tile they appear on, for `threshold` values 180, 210, 230 and 250. There are two intervals of particularly requent appearnance of hot spots, roughly between JPNs 84800 and 85500, and later between JPNs 86400 and 87500, which is in agreement with the frequency of the high temperature alarms (Fig. 1). The distribution of the hot spot appearance by divertor tiles, too, agrees with the alarms in Fig. 1, as in the first interval, most of the hot spots appear on tile 5, whereas in the second they appear on tiles 6 and 7., At all threshold values, the hot spots on tile 5 were detected in the beginning of the pulse range, which is consistent with the catalogue images, namely that the majority of detected hot spots on tile five originated from deliberately exposed surfaces (misaligned lamella, Langmuir probe tips) which were present on the surfaces of the tile from the beginning of the campaign. In contrast, the appearance of hot spots on tiles 6 and 7 was spread out more evenly throughout the pulse range, which would suggest that they were caused by the gradual degradation and/or contamination of the tile surfaces.

In general, as observed in the catalogue images, the number of newly appearing hot spots overall dropped with rising `threshold`, which is a rather obvious consequence of the algorithm functionality. In contrast to this trend, the pulse numbers of first appearance of hot spots on tile 6 are distributed relatively evenly throughout the pulse range at lower `threshold` values whereas at 250, the shape of the trend is significantly different, and more hot spots were first observed at a later pulse number (i.e. around 87000). This suggests that the activity of the hot spots increases over time. While the hot spots on tile 6 were active from e.g. JPN 86400 onwards, they became active enough to be registered at the highest threshold value only at around JPN 87000.

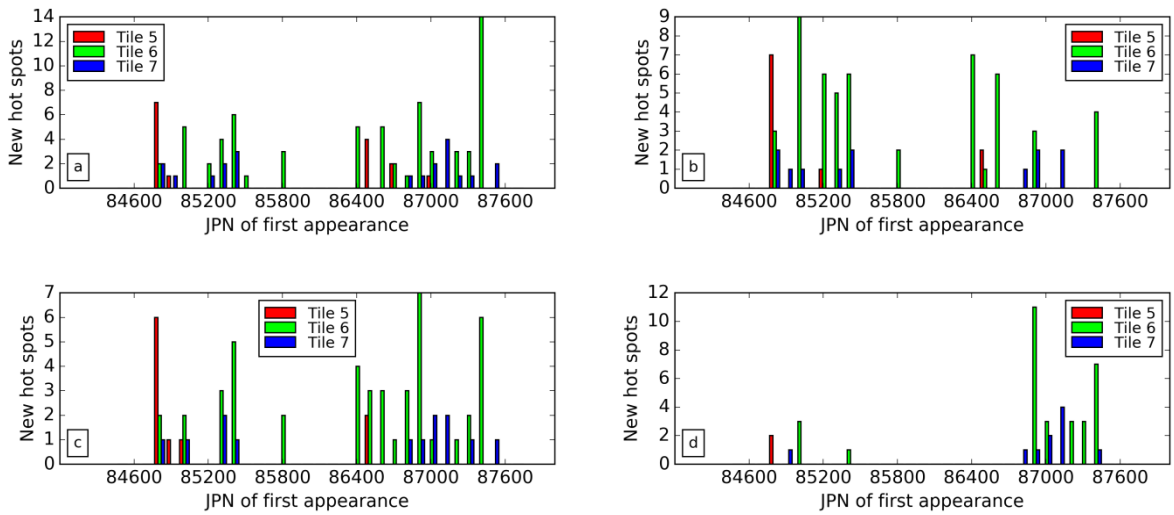

Figure 8. First noted hot spot activity in second run shown for each tile, for `threshold` values 180 (a), 210 (b), 230 (c) and 250 (d)

The dependence of the time of detection as a function of `threshold` can be decoupled from the total number of detected hot spots by plotting the fraction of hot spots which have been detected up to a certain pulse number, as shown in Fig 9, for each tile and several values of `threshold`. In line with Figs 7 and 8, the majority of the hot spots on tile 5 (Fig. 9a) were detected very early in the pulse range, although at lower `threshold` values, the fraction noted a slightly gradual increase. At the highest `threshold` setting, the almost only detected hot spot features on tile 5 were related to the misaligned lamella. Accordingly, they were all detected in a single event, and no additional hot spots were detected after that, which resulted in a very step-like shape of the fraction.

The detection of hot spots on tiles 6 (Fig. 9b) and 7 (Fig. 9c) was spread more evenly throughout the pulse range, however at the `threshold` values of 250, the majority of the hot spots were detected between pulse numbers 86800 and 87100. Again, this indicates at an increasing activity of the hot spots, which is also reflected in the frequency of high temperature alarms (Fig 1). On tile 7, the trend transitioned from early to late detection continuously with the rising `threshold` value, while on tile 6, the impact of the `threshold` value below 250 was slightly more scattered. Still, these results are in accordance with the interpretation of a gradual increase in the intensity of the hot spots on tiles 6 and 7.

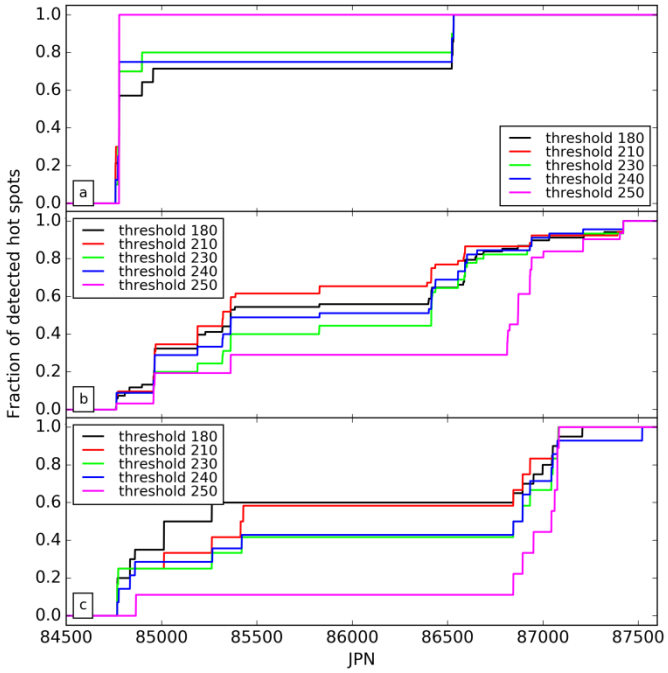

Figure 9. Fraction of detected hot spots (from the total catalogue entries) on tiles 5 (a), 6 (b) and 7 (c), for different `threshold` values

Defining the activation areas and minimum required NBI power for the activity of the hot spots makes it possible to distinguish whether the observed gradual increase in the hot spot activity was caused by gradually increasing powers deposited on unchanging plasma facing components, or was in indeed caused by changes on the surface. Thus, in each pulse we observe:

- *good time*: total time in which the outer strike point was within the defined activation area, and the NBI heating power was above the minimum value,
- *hot time*: the total time of hot spot activity within the good time intervals

The combined good and hot times are shown for the hot spots on tiles 6 and 7, detected at `threshold` value of 250 are shown in Figs 10a and 10b respectively. The quantities are combined for all hot spots which were first detected before, and after JPN 86000. This pulse number was chosen as it lies between the two major increases of the fraction of detected hot spots in Fig. 9, on both tiles.

Throughout the pulse range, the conditions for activity (Fig. 10 a, good time) of both groups of hot spots were met with a remarkably similar frequency, both in terms of absolute values as well as the trends, with the exception of a of a stretch between JPNs 87000 and 87200, where only the first group marked a dip in the trend. The trends of the hot spot activity (Fig. 10 b, hot time), were distinctly different between the two groups. The activity of the first group roughly followed the trends of the good time, while the second group, by definition, did not show any activity prior to JPN 86000. The difference in the good time was also visibly reflected in the stretch between JPNs 87000 and 87200.

The trends of the second group of hot spots indicate that they are indeed caused by changes on the plasma-facing surfaces, and not changes in plasma operation and the resulting plasma-facing interaction. The conditions for the activity of this particular group of hot spots were met with the same frequency as for the first one, well before it became active.

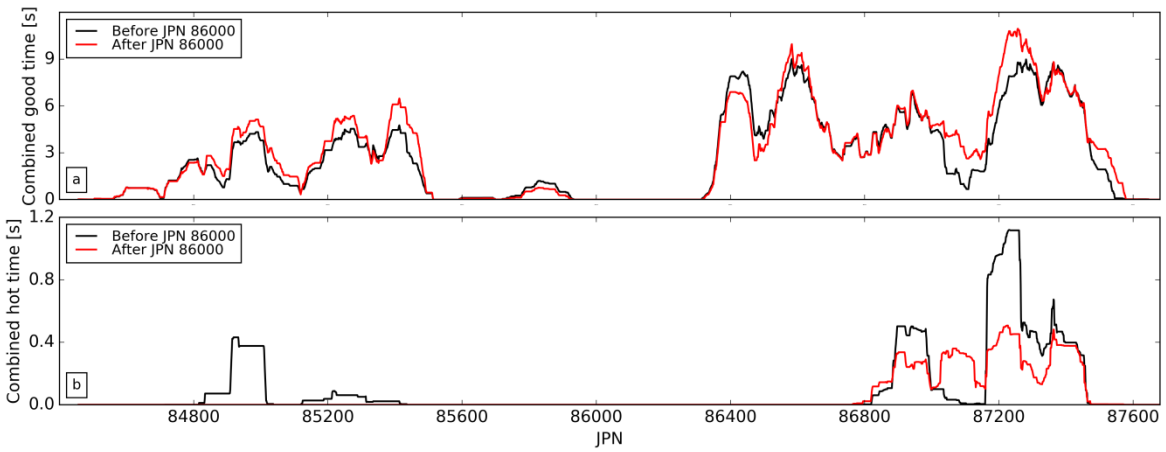

Figure 10. Rolling average (50-pulse wide) of the combined good time (a) and hot time (b), per pulse, for hot spots on divertor tiles 6 and 7 which were first detected before, and after JPN 86000, at the `threshold` value of 250

This interpretation is confirmed also with the same analysis performed at the threshold value of 180, shown in Fig 11. In this case, the pulse number that separates the two groups of hot spots was moved to JPN 85200, as this was the point before the biggest jump in the fraction of detected hot spots on both tiles (Fig. 9). With the lower threshold value, the hot time trends were found to follow the good trends more closely, however the main features of the results remain unchanged, i.e. the strike point had been in the collection area of the second group with the same frequency as for the first group, well before the second group showed any activity, and the significant increase in the activity of the second group in the range of pulses between JPN 87000 and 87200.

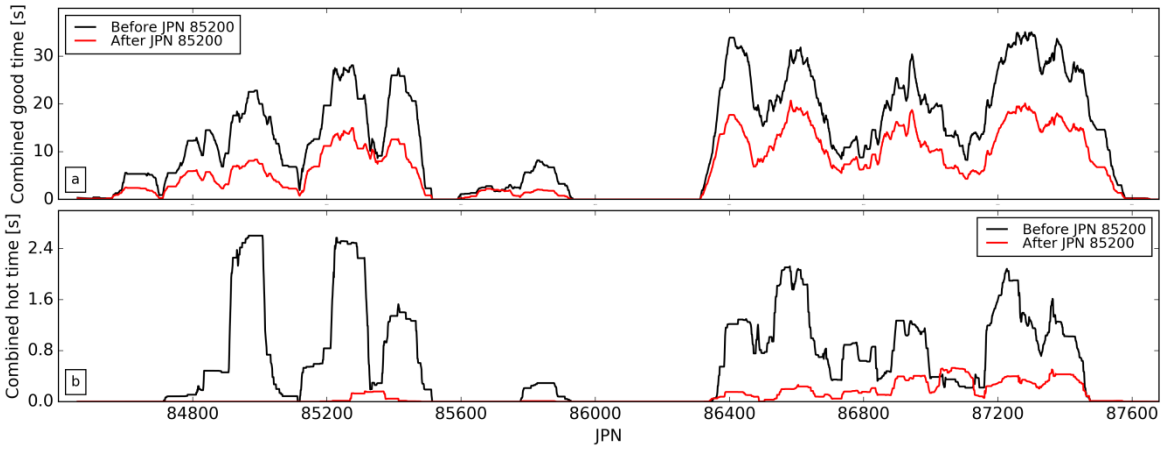

Figure 11. Rolling average (50-pulse wide) of the combined good time (a) and hot time (b) for hot spots on divertor tiles 6 and 7 which were first detected before, and after JPN 82000, at the `threshold` value of 180

The activation areas of the majority of the hot spots on tiles 6 and 7 were smaller than 5 cm, as seen in Fig. 12, which is consistent with the characteristics expected from hot spots, i.e. that their activity is triggered when the strike point is within a narrow strip on the divertor tiles. At lower `threshold` values, the distribution was extended to a small number of hot spots with a larger activation size (8 cm), which is likely less consistent with hot spot behaviour.

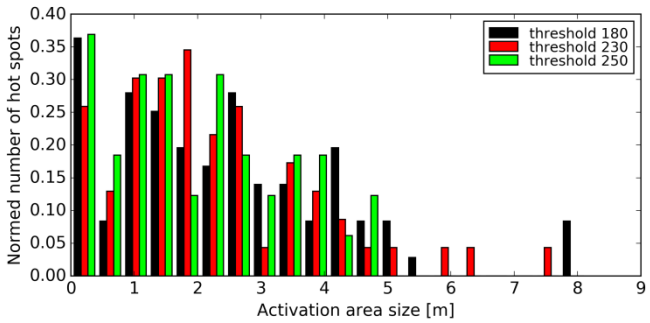

Figure 12. Normed distribution of the size of activation areas of hot spots on tiles 6 and 7 at the `threshold` values of 180, 210, 230, 240 and 250 (b)

4. Conclusions

In support of analysis of hot spots, observed with the protection cameras at JET, a method of automated hot spot detection, recognition and analysis was developed. The method is based on a relatively simple image analysis process which identifies isolated clusters of bright pixels in the raw camera images, their recognition during the course of the video recording, and the analysis of their temporal behaviour. It is controlled by four parameters, i.e. the image binarisation threshold for separating bright and dark pixels, the required persistence of the hot pixel clusters, and two parameters which control the recognition of the clusters.

The performance of the method was tested in a limited pulse range, which allowed for the selection of optimal values of the recognition and persistence parameters, and a range of the values of the threshold in which the algorithm did not label any obviously non-hot spot features (i.e. large illuminated areas) as hot spots.

The appearance and activity of the hot spots was analysed in the recordings of the KL1-P4DB protection camera, looking at the outer divertor, in the 2nd ILW campaign. Recognizing the hot spots in different frames of the video recording allows for tracking of their activity throughout the whole pulse range and this, in turn, allows for relating their activity to the position of the outer strike point, and the NBI heating power.

The properties of the features, detected by the method of analysis, corresponded to hot spots – beside their appearance in the camera images, their activity was triggered when the outer strike point was within a narrow (few cm wide) strip. The behaviour of the hot spots detected on tile 5, as well as their visual observation in the camera images, indicated that they were predominantly related to deliberately exposed surfaces (a misaligned divertor lamella and Langmuir probe tips), whereas the hot spots detected on tiles 6 and 7 were more likely to related to the gradual degradation and/or contamination of the plasma-facing surfaces. In contrast to the tile 5 hot spots which were detected shortly after the start of the campaign, the tile 6 and 7 hot spots were appearing throughout the whole analysed pulse range. The appearance and activity of the detected hot spots were in accordance to the high temperature alarms triggered by the thermal protection system in the same pulse range. The observation of the gradual appearance of the tile 6 and 7 hot spots was made possible by varying the image binarisation threshold. While the recognition becomes less accurate at lower threshold values, the results are still relevant as the hot spots of low intensity can be detected before their intensity increases to the point of triggering high temperature alarms in the thermal protection system in later pulses. The interpretation that the gradual appearance of hot spots was caused by changes on the tile surfaces, and not changes in the plasma operation, was confirmed by the fact that the conditions for activity of a significant part of the tile 6 and 7 hot spots was frequently met well before their first activity.

The developed algorithm for detection of hot spots in the protection camera recording is planned to be integrated into the software suite in use by the visual systems operators at JET[11]. Beyond that, the analysis of the activity of the hot spots during a running campaign can be used to help to identify potential hot spots before they evolve to the point of prematurely terminating pulses by causing high temperature alarms, while the identified plasma parameter values can serve as input data for shaping future discharges to avoid further degradation of the divertor surfaces.

5. Acknowledgements

This work has been carried out within the framework of the EUROfusion Consortium and has received funding from the Euratom research and training programme 2014-2018 under grant agreement No 633053. The views and opinions expressed herein do not necessarily reflect those of the European Commission.

6. References

[1] F. Romanelli, M. Abhangi, P. Abreu, M. Aftanas, J.E.T. Contributors, et al., Overview of the JET results, Nucl. FUSION. 55 (2015). doi:10.1088/0029-5515/55/10/104001.

[2] V. Riccardo, M. Firdaouss, E. Joffrin, G. Matthews, P. Mertens, V. Thompson, E. Villedieu, Operational limits for the ITER-like wall in JET, Phys. Scr. T138 (2009). doi:10.1088/0031-8949/2009/T138/014033.

[3] H. Maier, R. Neu, H. Greuner, B. Boeswirth, M. Balden, S. Lindig, G.F. Matthews, M. Rasinski, P. Wienhold, A. Wiltner, Qualification of tungsten coatings on plasma-facing components for JET, Phys. Scr. T138 (2009). doi:10.1088/0031-8949/2009/T138/014031.

[4] P. Mertens, V. Philipps, G. Pintsuk, V. Riccardo, U. Samm, V. Thompson, I. Uytdenhouwen, Clamping of solid tungsten components for the bulk W divertor row in JET-precautionary design for a brittle material, Phys. Scr. T138 (2009). doi:10.1088/0031-8949/2009/T138/014032.

[5] G. Arnoux, S. Devaux, D. Alves, I. Balboa, C. Balorin, N. Balshaw, M. Beldishevski, P. Carvalho, M. Clever, S. Cramp, J.-L. de Pablos, E. de la Cal, D. Falie, P. Garcia-Sanchez, R. Felton, V. Gervaise, A. Goodyear, A. Horton, S. Jachmich, A. Huber, M. Jouve, D. Kinna, U. Kruezi, A. Manzanares, V. Martin, P. McCullen, V. Moncada, K. Obrejan, K. Patel, P.J. Lomas, A. Neto, F. Rimini, C. Ruset, B. Schweer, G. Sergienko, B. Sieglin, A. Soleto, M. Stamp, A. Stephen, P.D. Thomas, D.F. Valcarcel, J. Williams, J. Wilson, K.-D. Zastrow, J.-E. Contributors, A protection system for the JET ITER-like wall based on imaging diagnostics, Rev. Sci. Instrum. 83 (2012). doi:10.1063/1.4738742.

[6] V. Huber, A. Huber, D. Kinna, I. Balboa, S. Collins, N. Conway, P. Drewelow, C.F. Maggi, G.F. Matthews, A.G. Meigs, P. Mertens, M. Price, G. Sergienko, S. Silburn, A. Wynn, K.-D. Zastrow, In-vessel calibration of the imaging diagnostics for the real-time protection of the JET ITER-like wall, Rev. Sci. Instrum. 87 (2016). doi:10.1063/1.4959912.

[7] A. Huber, D. Kinna, V. Huber, G. Arnoux, I. Balboa, C. Balorin, P. Carman, P. Carvalho, S. Collins, N. Conway, P. McCullen, S. Jachmich, M. Jouve, C. Linsmeier, B. Lomanowski, P.J. Lomas, C.G. Lowry, C.F. Maggi, G.F. Matthews, T. May-Smith, A. Meigs, P. Mertens, I. Nunes, M. Price, P. Puglia, V. Riccardo, F.G. Rimini, G. Sergienko, M. Tsalas, K.-D. Zastrow, J.E.T. Contributors, The near infrared imaging

system for the real-time protection of the JET ITER-like wall, Phys. Scr. T170 (2017). doi:10.1088/1402-4896/aa8a14.
[8] A. Huber, D. Kinna, V. Huber, G. Arnoux, G. Sergienko, I. Balboa, C. Balorin, P. Carman, P. Carvalho, S. Collins, N. Conway, P. Mccullen, A. Drenik, S. Jachmich, M. Jouve, C. Linsmeier, B. Lomanowski, P.J. Lomas, C.G. Lowry, C.F. Maggi, G.F. Matthews, A. Meigs, P. Mertens, I. Nunes, M. Price, P. Puglia, V. Riccardo, F.G. Rimini, A. Widdowson, K.-D. Zastrow, J.E.T. Contributors, Real-time protection of the JET ITER-like wall based on near infrared imaging diagnostic systems, Nucl. FUSION. 58 (2018). doi:10.1088/1741-4326/aad481.
[9] D.F. Valcarcel, D. Alves, P. Card, B.B. Carvalho, S. Devaux, R. Felton, A. Goodyear, P.J. Lomas, F. Maviglia, P. McCullen, C. Reux, F. Rimini, A. Stephen, L. Zabeo, K.-D. Zastrow, J.E. Contributors, The JET real-time plasma-wall load monitoring system, FUSION Eng. Des. 89 (2014) 243–258. doi:10.1016/j.fusengdes.2013.10.010.
[10] V. Rohde, M. Balden, T. Lunt, A.U. Team, Dust investigations at ASDEX Upgrade, Phys. Scr. T138 (2009). doi:10.1088/0031-8949/2009/T138/014024.
[11] V. Huber, A. Huber, D. Kinna, G. Matthews, I. Balboa, A. Capel, P. McCullen, P. Mertens, G. Sergienko, S. Silburn, K.-D. Zastrow, JUVIL: A new innovative software framework for data analysis of JET imaging systems intended for the study of plastha physics and machine operational safety, FUSION Eng. Des. 123 (2017) 979–985. doi:10.1016/j.fusengdes.2017.03.005.
[12] K. Madkour, S. Mohamed, D. Tantawy, M. Anis, Hotspot Detection using Machine Learning, in: Proc. SEVENTEENTH Int. Symp. Qual. Electron. Des. ISQED 2016, IEEE, 345 E 47TH ST, NEW YORK, NY 10017 USA, 2016: pp. 405–409.
[13] V. Martin, J.-M. Travere, V. Moncada, F. Bremond, Towards Intelligent Video Understanding Applied to Plasma Facing Component Monitoring, Contrib. PLASMA Phys. 51 (2011) 252–255. doi:10.1002/ctpp.201000054.
[14] V. Martin, J.-M. Travere, F. Bremond, V. Moncada, G. Dunand, Thermal Event Recognition Applied to Protection of Tokamak Plasma-Facing Components, IEEE Trans. Instrum. Meas. 59 (2010) 1182–1191. doi:10.1109/TIM.2009.2038032.
[15] T. Craciunescu, A. Murari, B. Sieglin, G. Matthews, J.E. Contributors, An Original Method for Spot Detection and Analysis for Large Surveys of Videos in JET, IEEE Trans. PLASMA Sci. 42 (2014) 1358–1366. doi:10.1109/TPS.2014.2311463.
[16] J.W. Coenen, G. Arnoux, B. Bazylev, G.F. Matthews, S. Jachmich, I. Balboa, M. Clever, R. Dejarnac, I. Coffey, Y. Corre, S. Devaux, L. Frassinetti, E. Gauthier, J. Horacek, M. Knaup, M. Komm, K. Krieger, S. Marsen, A. Meigs, P. Mertens, R.A. Pitts, T. Puetterich, M. Rack, M. Stamp, G. Sergienko, P. Tamain, V. Thompson, J.-E. Contributors, ELM induced tungsten melting and its impact on tokamak operation, J. Nucl. Mater. 463 (2015) 78–84. doi:10.1016/j.jnucmat.2014.08.062.
[17] G.F. Matthews, B. Bazylev, A. Baron-Wiechec, J. Coenen, K. Heinola, V. Kiptily, H. Maier, C. Reux, V. Riccardo, F. Rimini, G. Sergienko, V. Thompson, A. Widdowson, J.E.T. Contributors, Melt damage to the JET ITER-like Wall and divertor, Phys. Scr. T167 (2016). doi:10.1088/0031-8949/T167/1/014070.
[18] K. Heinola, A. Widdowson, J. Likonen, E. Alves, A. Baron-Wiechec, N. Barradas, S. Brezinsek, N. Catarino, P. Coad, S. Koivuranta, S. Krat, G.F. Matthews, M. Mayer, P. Petersson, J.E.T. Contributors, Long-term fuel retention in JET ITER-like wall, Phys. Scr. T167 (2016). doi:10.1088/0031-8949/T167/1/014075.